Scientia Iranica D (2014) 21(6), 2200–2212

SCIENTIA IRANICA

Sharif University of Technology
Scientia Iranica
Transactions D: Computer Science & Engineering and Electrical Engineering
www.scientiairanica.com

Investigating performance of the new FC-MCR compensator for enhancing power system stability using multi-objective Imperialist Competitive Algorithm (ICA)

R. Ghanizadeh[a,*], M. Ebadian[a], M.A. Golkar[b] and A. Jahandideh Shendi[c]

a. *Faculty of Electrical and Computer Engineering, University of Birjand, Birjand, Iran.*
b. *Faculty of Electrical and Computer Engineering, K.N. Tossi University of Technology, Tehran, Iran.*
c. *Faculty of Electrical Engineering, Islamic Azad University, Shabestar Branch, Iran.*

Received 28 December 2012; received in revised form 10 November 2013; accepted 25 January 2014

KEYWORDS
Magnetically Controlled Reactor with Fixed Capacitor banks (FC-MCR);
Power system dynamic stability;
Imperialist Competitive Algorithm (ICA).

Abstract. In this paper, a novel compensator based on a Magnetically Controlled Reactor with Fixed Capacitor banks (FC-MCR) is introduced and, then, power system stability, in the presence of this compensator, has been studied using an intelligent control method. The problem of the robust FC-MCR based damping controller design is formulated as a multi-objective optimization problem. The multi-objective problem is concocted to optimize a composite set of two eigenvalue-based objective functions comprised of the desired damping factor, and the desired damping ratio of the lightly damped and undamped electromechanical modes. The controller is automatically tuned with optimization of an eigenvalue based multi-objective function by ICA to simultaneously shift the lightly damped and undamped electromechanical modes to a prescribed zone in the s-plane, so that relative stability is guaranteed and time domain specifications concurrently secured. The effectiveness of the proposed controller is demonstrated through eigenvalue analysis, nonlinear time simulation studies and some performance indices to damp low frequency oscillations under different operating conditions. The results show that the tuned ICA based FC-MCR controller, which is designed using the proposed multi-objective function, has an outstanding capability for damping power system low frequency oscillations and significantly improves the power systems dynamic stability.

1. Introduction

The main priorities in a power system operation are its security and stability. Thus, a control system should maintain its frequency and voltage at a fixed level against any kind of disturbance, including a sudden increase in load, a generator being out of circuit, or the failure of a transmission line due to human error, technical defects, natural disasters, etc. Due to the new legislations of the electricity market, this situation creates double stress for beneficiaries [1,2]. Low frequency oscillations that are in the range of 0.2 to 3 Hz are created by the development of large power systems and their connections. These oscillations continue to exist in the system for a long time and if not well-damped, the amplitudes of these oscillations increase and bring about the isolation and instability of the system [3-5]. Using a Power System Stabilizer (PSS) is technically

*. *Corresponding author. Tel.: +98 561 2202203; Fax: +98 561 2227795*
E-mail addresses: r_ghanizadeh@birjand.ac.ir (R. Ghanizadeh); mebadian@birjand.ac.ir (M. Ebadian); Golkar@kntu.ac.ir (M.A. Golkar); ajahandide64@gmail.com (A. Jahandideh shendi)

and economically appropriate for damping oscillations and increasing the stability of a power system. Various methods have been proposed for designing these stabilizers [6-8]. Hhowever, these stabilizers cause the power factor to become leading and, therefore, have a major disadvantage leading to loss of stability caused by large disturbances, particularly, a three phase fault at the generator terminals [9]. In recent years, the use of Flexible Alternating Current Transmission Systems (FACTS) has been proposed as an effective method for improving system controllability and the limitations of power transfer. By modeling the bus voltage and phase shift between buses and the reactance of transmission lines, FACTS controllers can cause increments in the power transfer in steady state. These controllers are added to a power system for controlling normal steady state. But, because of their rapid response, they can also be used for improving power system stability through damping the low frequency oscillations [1-6,10].

The Static Var Compensator (SVC) is a member of the FACTS devices family which is connected in parallel to the system. These compensators have a faster response, and better stability control, etc. [11-13]. In spite of their advantages, these compensators also have some disadvantages, including high THD and high maintenance costs [14-16]. Also, these compensators need a step-down transformer to make network voltage less than 35 KV and, at the same time, require the use of lots of power electronic elements, both in series and in parallel, which increase loss and the cost of these compensators [17].

MCRs are powerful low-inertia inductors, in which reactive power consumption can be regulated from 0.01 to 1.0 times the rated power with short term regulation (up to 1 min) up to 2.0 times the rated power. Because of this very wide range of control, MCRs reduce idle-mode power losses significantly. They also increase the operational reliability of electrical grids and optimize power line operating conditions. MCRs increase power quality through automatic voltage regulation, reduced fluctuation, smoothing of reactive power surges, damping voltage oscillation, increasing power stability limits and permitting higher voltage transmissions [17-19].

The MCR is controlled by changing the magnetic permeability of the core. Magnetization of the steel is controlled by a DC current in the control windings of the reactor, thus, achieving the magnetic biasing of the steel. MCR is based on two original principles:

1. The first principle of the MCR is the generation and control of the direct component of the magnetic flux in the MCR's two cores by periodic shorting of some reactor winding turns using semiconductor switches [18].
2. The second principle of the MCR is profound magnetic saturation of the two cores under rated conditions, when the saturation magnetization is generated by about half or more of the grid frequency period [14].

In this paper, the modified linearized Phillips-Heffron model is utilized to theoretically analyse a Single-Machine Infinite-Bus (SMIB) installed with FC-MCR. Then, the results of this analysis is used for assessing the potential of an FC-MCR supplementary controller to improve the dynamic stability of a power system. The issue of designing a robust FC-MCR-based controller is considered and formulated as an optimization problem, according to the eigenvalue-based multi-objective function, consisting of the damping ratio of the undamped electromechanical modes. Next, considering its high capability to find the most optimistic results, the Imperialist Competitive Algorithm (ICA) is used to solve this optimization problem. A wide range of operating conditions are considered in the design process of the proposed damping controller in order to guarantee its robustness. The effectiveness of the proposed controller is demonstrated through eigenvalue analysis, controllability measures, nonlinear time-domain simulation and some performance indices studies. Evaluation results show that the proposed multi-objective function based tuned damping controller achieves good robust performance under a wide range of operating conditions and is superior to both controllers designed using the single objective functions.

The rest of this paper is organized as follows, in Section 2 of this paper, the imperialist competitive algorithm is introduced. In Section 3, the MCR theory is fully described. In Section 4, the nonlinear model of a Single-Machine Infinite-Bus (SMIB) system in the presence of FC-MCR is presented and equations are thoroughly extracted. In Section 5, the robust controller design using a multi-objective ICA algorithm is presented. Finally, the robustness of the controller, eigenvalue analysis and nonlinear simulation of different modes of the system are presented. The last section concludes the paper.

2. Imperialist Competitive Algorithm (ICA)

In recent decades, intelligent optimization algorithms, that are inspired by nature, have shown great success. Among these methods, we can name genetic algorithms (inspired by the evolution of species), ant colony optimization (based on the optimal movement of ants) and particle swarm optimization (inspired by the mass movement of birds and fish). Many of these methods have been used for solving optimization problems in various fields. Recently, a new optimization algorithm, called the imperialist competitive algorithm, has been presented by Lucas, which is inspired by a social phenomenon rather than nature [20].

The innovators of this algorithm analyzed the historical phenomenon of colonialism, in line with the social-political development in human societies and, then, by mathematical modeling of this process, they presented a powerful optimization algorithm. The results obtained after applying this algorithm to various fields of electrical, computer, industrial, mechanical engineering, etc., have shown its effectiveness in solving optimization problems. The high performance and innovative aspects of this algorithm make it attractive for optimization domain experts [21].

In order to have a better understanding of the behavior of the Imperialist Competitive Algorithm (ICA), its performance is described by comparing it with the Genetic Algorithm (GA). In genetic algorithms, there is a population that consists of several individuals. By applying crossover, mutation and selection operators to the population, the algorithm is led towards better results in the search space. The selection of parents and children for the next generation is based on the fitness of each individual. In ICA there are some countries which correspond to individuals in the Genetic Algorithm (GA). In fact, this set of countries is a set of random points within the search space. Then, some more powerful countries (which have higher fitness values) are selected as imperialists. The powerful countries are selected as imperialists and weak countries as colonies [22]. At the beginning of the algorithm, countries are generated randomly and a few powerful countries are selected as imperialists. Then, other countries are randomly assigned to one of the imperialists (Figure 1). The number of colonies of imperialists is proportional to their power. As shown in Figure 1, stronger imperialists (bigger stars) allocated more colonies to themselves.

By applying an assimilation policy, imperialist countries attract heir colonies to themselves along different axes, such as language and culture [23]. This

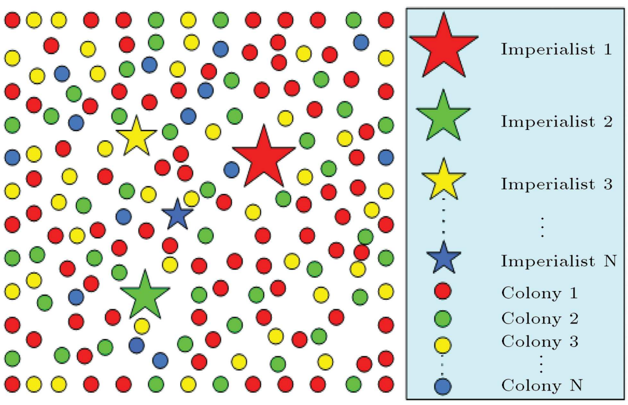

Figure 1. Initial produced imperialists and their colonies.

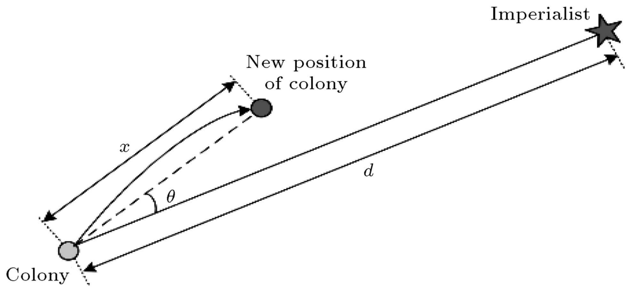

Figure 2. Movement of colonies toward their related imperialist.

issue is modeled with the random motion of each colonial country to its imperialist country, in the search space. As shown in Figure 2, moving the colony country towards the imperialist country is done by the size of x and the deviation angle, θ. These values are assigned randomly, and can be obtained from Eq. (1) [24]:

$$x \approx U(0, \beta \times d), \qquad \theta \approx U(-\gamma, \gamma). \tag{1}$$

In the the above equation, the terms β and γ describe parameters that modify the area in which the imperialist randomly searches around the colonies.

In the countries moving process throughout the algorithm, a colony country may get more power than an imperialist country. Under this condition, imperialists and colonial countries would exchange places at the next levels. In other words, all colonial countries of a previously imperialist country will belong to the new imperialist country, and these colonies will move towards the new imperialists. At each step of the iteration of the algorithm, there is competition between imperialists. In this competition, the imperialist which has less power than other imperialists loses one of its colonies. In this process, the weakest colonial of the weakest imperialists joins one of the other imperialists. The possibility of assigning this new colony to other imperialists is proportional to the amount of their power. If one imperialist loses all its colonies, it would become a colony of another imperialist [21].

The algorithm continues until the number of imperialists reaches one. In this case, all colony countries belong to a single imperialist and the algorithm ends. Of course, other stopping criteria, such as the number of iterations, can be applied; in this condition the flowchart of colonial competition would be similar to Figure 3. This algorithm is explained in more details in [20,21].

3. Theory of MCR

3.1. MCR

The elementary MCR is represented in Figure 4 [14,18]. The W_1 windings are placed in an AC circuit having

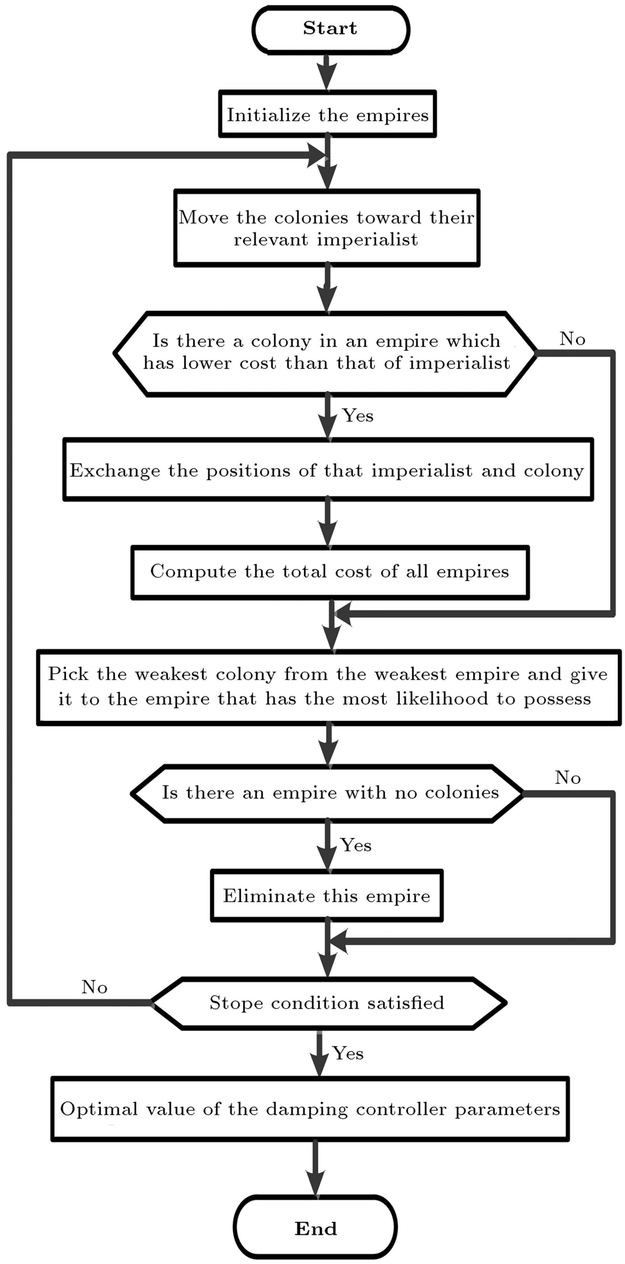

Figure 3. Flowchart of Imperialist Competitive Algorithm (ICA).

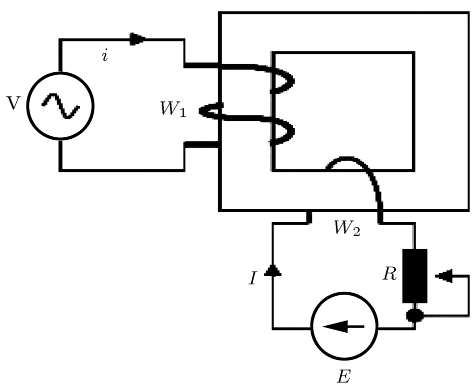

Figure 4. The elementary controlled inductance.

an alternating current (i), while controlled by the W_2 windings, which are joined to a DC source. If $\varphi = \varphi_m \sin(wt)$ and $\varphi = f(HL)$, then, for each value of W_2 with curve $[f = f(Hl)]$, appropriate values of (HL) are found and a curve is built $[f(wt) = iw_1 + Iw_2]$.

If the DC voltage in the W_2 windings is zero, then, the current in the W_2 windings will be zero. In this state, the current of the W_2 windings will produce sinusoidal flux, and the reactor current will be sinusoidal. Figure 5(a) shows magnetic flux and current when $I = 0$. If the DC voltage in the W_2 windings is not zero, then the current in the W_2 windings will not be zero. In this state, the DC voltage produces constant flux (φ_0), and the total flux will be $\varphi = \varphi_m \sin(wt) + \varphi_0$. Figure 5(b) shows the magnetic flux and current when $I \neq 0$. Note that current i does not contain a constant component, as in the circuit of W_1 windings, there is no source of DC.

The line A_1-A_2 in Figure 5(b) would be a zero line for curve $iw_1 = f(wt)$. The current of the W_2 windings changes about this straight line, so, the average current for the period of $wt = 0$ to $wt = 2\pi$ is equal to zero.

3.2. Basic electric circuits of MCR

The basic electrical circuit of MCRs is shown in Figure 6(a) [14-19], which is the basic idealized circuit for connecting the windings of the two cores in which the single-phase coincides with one of the widespread circuits of the magnetic amplifiers (Figure 6(a)). There are two closed magnetic circuits each of which is covered with half of each winding, CO and OY. The parts of the OY windings are connected consistently, and with current in CO windings, one has the same direction and another has the opposite direction (Figure 6(a)). Figure 6(b) shows the current in the CO windings at the voltage source (E) in OY windings. Under normal conditions ($E = 0$), the MCR is not saturated. With an increase in voltage, E, the current of the MCR (i) in the W_1 windings (Figure 4) increases from zero to maximum, and the reactive power consumed in the reactor also increases. The current is essentially reactive and sinusoidal.

4. Description of case study system

Figure 7 shows a Single-Machine Infinite-Bus (SMIB) power system equipped with an FC-MCR. The synchronous generator is delivering power to the infinite-bus through a double circuit transmission line and an FC-MCR. The parameters of the test power system are given in the Appendix.

4.1. Power system nonlinear model with FC-MCR

A single-line schematic diagram of FC-MCR compensator is shown in Figure 8. The FC-MCR consists of (1) MCR reactor, (2) capacitor bank, (3) three-

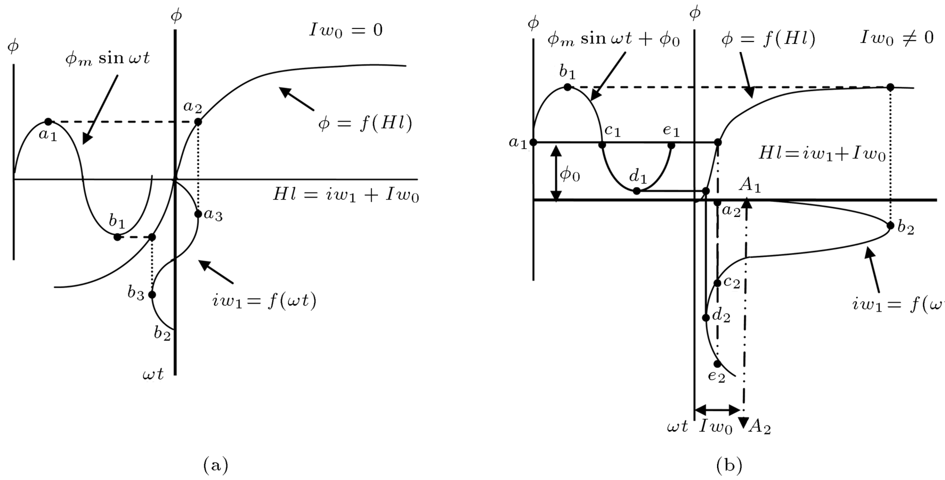

Figure 5. Magnetic flux and current when (a) $I = 0$, and (b) $I \neq 0$.

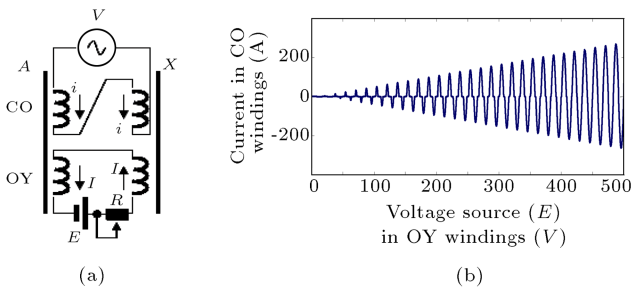

Figure 6. (a) The basic electrical circuits of MCR. (b) Current in CO windings at the voltage source E in OY windings.

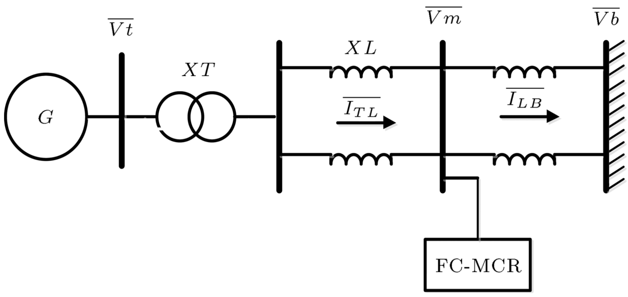

Figure 7. SMIB power system equipped with FC-MCR.

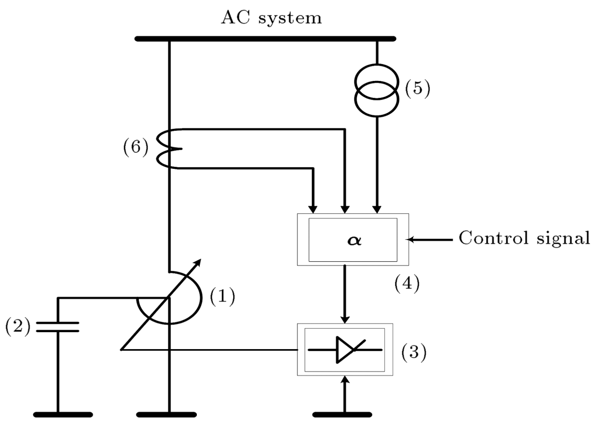

Figure 8. Single-line circuit of FC-MCR compensator.

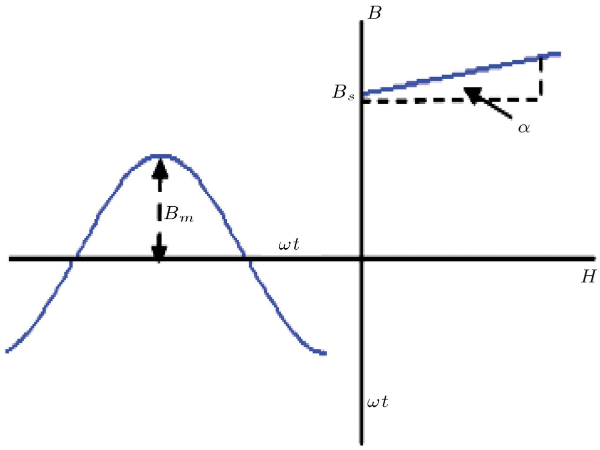

Figure 9. Flux and current curves of the reactor when DC voltage is zero.

phase transformers with built-in thyristor converters for producing the DC voltage, (4) control, safety, and automation system for FC-MCR, (5) voltage transformer, and (6) current transformer.

Since the FC-MCR is similar to a conventional transformer, to obtain the current equation, the performance of this compensator is investigated in two cases. In the first case, if the DC voltage applied to the FC-MCR is zero, no constant flux is added to the main flux and, consequently, the current of FC-MCR will be zero. Figure 9 shows the flux and current curves of FC-MCR when the DC voltage is zero. According to Figure 9, it can be concluded that:

$$\varphi = 180,$$

$$\sigma = 2(\pi - \varphi) = 0 \ \Rightarrow I_{\text{reactor}} = 0.$$

In the second case, the DC voltage applied to the FC-MCR is not zero. This voltage generates a constant flux. Consequently, this flux is added to the main flux and, as a result of the intersection with the magnetic saturation curve, it generates the current

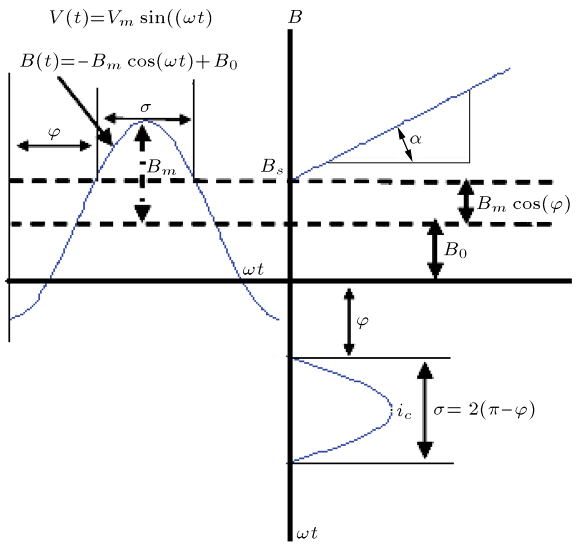

Figure 10. Flux and current curves of the reactor when DC voltage is not zero.

of the compensator. Figure 10 shows the flux and current curves of the FC-MCR compensator when the DC voltage is not zero.

According to Figure 10, the value of the magnetic flux density can be represented by:

$$B(t) = B_m \cos(\omega t) + B_0. \tag{2}$$

The relationship between magnetic flux density (B) and magnetic field strength is indicated in Figure 10. It is realized from Figure 10 that for a positive half-wave, the magnetic field strength can be represented by Eq. (3):

$$H = \begin{cases} Hm\,(\cos(\varphi) - \cos(\omega t)) & \varphi < \omega t < 2\pi - \varphi \\ 0 & 2\pi - \varphi < \omega t < \varphi + \pi \end{cases} \tag{3}$$

where:

$$H_m = B_m \cot(\alpha) = B_m \frac{1}{\tan(\alpha)} = \frac{\phi_m}{s} \cot(\alpha)$$

$$= \frac{V_m}{s.\omega} \cot(\alpha). \tag{4}$$

According to Eqs. (3) and (4), the current equation of FC-MCR can be obtained as:

$$I = \begin{cases} I_m\,(\cos(\varphi) - \cos(\omega t)) & \varphi < \omega t < 2\pi - \varphi \\ 0 & 2\pi - \varphi < \omega t < \varphi + \pi \end{cases} \tag{5}$$

where:

$$I_m = H_m l = B_m l \cot(\alpha) = \frac{\phi_m}{S} l \cot(\alpha) = \frac{V_m.l}{s.\omega} \cot(\alpha). \tag{6}$$

In the above equation, α is the angle that is effective in the MCR current and dependent on the core characteristic, and S is the cross-section area of the core.

The fundamental harmonic of FC-MCR current can be obtained using Fourier analysis.

$$I = \frac{V.l}{\pi \omega s} \tan(\alpha)\,(2(\pi - \varphi) - \sin(2(\pi - \varphi)))\,, \tag{7}$$

where φ is the angle due to DC voltage.

Considering the following equation, the FC-MCR susceptance equation can be obtained:

$$I = B_c(\alpha).V. \tag{8}$$

Thus:

$$B_c(\varphi) = \frac{1}{X_c} - \frac{1}{\pi X_L}\,(2(\pi - \varphi) - \sin(2(\pi - \varphi)))\,. \tag{9}$$

In Eq. (9), $B_C(\varphi)$ is the adjustable susceptance in the fundamental frequency and it is controlled by the angle generated by the DC voltage. Figure 11 shows the susceptance variation curve of FC-MCR with changes in φ.

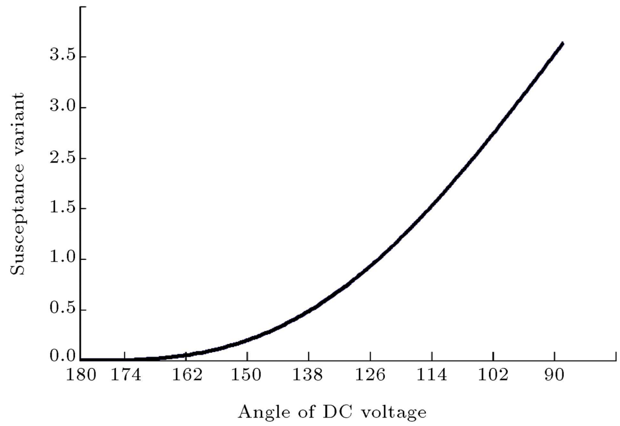

Figure 11. Susceptance variation curve of FC-MCR with changes in φ.

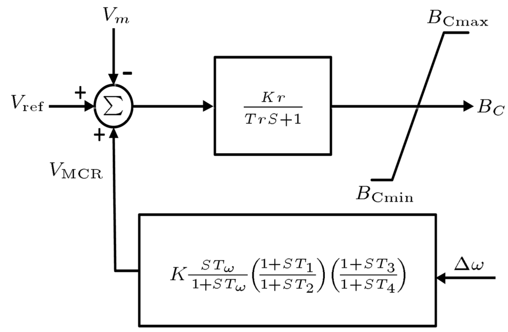

Figure 12. Control block diagram of FC-MCR.

Considering the investigated cases, the FC-MCR compensator can be modeled by a first order dynamic equation with acceptable precision. Figure 12 shows the control block diagram of FC-MCR.

According to Figure 12, it can be written:

$$\frac{K_r}{T_r S+1}\left(V_{\mathrm{ref}}-V_m+V_{\mathrm{MCR}}\right)=B_C. \qquad (10)$$

Eq. (10) can be written as follows:

$$\dot{B}_C=-\frac{1}{T_r}B_C+\frac{K_r}{T_r}\left(V_{\mathrm{ref}}-V_m+V_{\mathrm{MCR}}\right), \qquad (11)$$

where B_C is susceptance, and K_r and T_r are the gain and time constants considered for thyristor firing angles.

The nonlinear model of the SMIB system, as shown in Figure 7, is described by [1]:

$$\dot{\delta}=\omega_\circ(\omega-1), \qquad (12)$$

$$\dot{\omega}=\frac{1}{M}\left(P_m-P_e-D\Delta\omega\right), \qquad (13)$$

$$\dot{E'}_q=\frac{1}{T'_{\mathrm{do}}}\left(E_{fd}-E_q\right), \qquad (14)$$

$$\dot{E}_{fd}=-\frac{1}{T_A}E_{fd}+\frac{K_A}{T_A}\left(V_{\mathrm{ref}}-V_t\right), \qquad (15)$$

where:

$$P_e=E'_qI_q+\left(X_q-X'_d\right)I_dI_q,$$

$$E_q=E'_q+\left(x_d-x'_d\right).I_d,$$

$$V_t=\sqrt{(X_qI_q)^2+(E'_q-X'_dI_q)^2},$$

$$V_m=\sqrt{\left(E'_q-(X'_d+X_{L1}+X_T)I_d\right)^2+\left((X_q+X_{L1}+X_T)I_q\right)^2},$$

$$I_d=\frac{E'_q(1-X_{L2}B_C)}{X_D}-\frac{V_b\cos(\delta)}{X_D},$$

$$I_q=-\frac{V_b\sin(\delta)}{X_Q},$$

$$X_D=\left(X'_d+X_{L1}+X_T+X_{L2}\right)-\left(X'_d(X_{L1}+X_T)+(X_{L1}+X_T)X_{L2}\right),$$

$$X_Q=-\left(X'_q+X_{L1}+X_T+X_{L2}\right)+\left(X'_q(X_{L1}+X_T)+(X_{L1}+X_T)X_{L2}\right).$$

4.2. Power system linearized model

A linear dynamic model is obtained by linearizing the nonlinear model round an operating condition. The linearized model of the power system, as shown in Figure 7, is given as follows:

$$\Delta\dot{\delta}=\omega_\circ.\Delta\omega, \qquad (16)$$

$$\Delta\dot{\omega}=\frac{1}{M}\left(\Delta T_m-K_1.\Delta\delta-K_2.\Delta e'_q-K_3.\Delta B_C-kd.\Delta\omega\right), \qquad (17)$$

$$\Delta\dot{E'}_q=\frac{1}{T'_{\mathrm{do}}}\left(\Delta E_{fd}+K_4.\Delta\delta+K_5.\Delta E'_q+K_6.\Delta B_C\right), \qquad (18)$$

$$\Delta\dot{E}_{fd}=-\frac{1}{T_A}\Delta E_{fd}+\frac{K_A}{T_A}\times\left(\Delta V_{\mathrm{ref}}-K_7.\Delta\delta-K_8.\Delta E'_q-K_9.\Delta B_C\right), \qquad (19)$$

$$\Delta\dot{B}_C=-\frac{1}{T_r}\Delta E_{fd}+\frac{K_r}{T_r}\times\left(-K_{10}.\Delta\delta-K_{11}.\Delta e'_q-K_{12}.\Delta B_C+\Delta\omega\right), \qquad (20)$$

where, $K_1, K_2, ..., K_{12}$ are linearization constants. The system state space model is obtained as follows:

$$\dot{X}=Ax+Bu, \qquad (21)$$

where, x is the state vector, u is the control vector, and A and B are:

$$\begin{bmatrix}\Delta\dot{\delta}\\ \Delta\dot{\omega}\\ \Delta\dot{E'}_q\\ \Delta\dot{E}_f\\ \Delta\dot{B}_C\end{bmatrix}=\begin{bmatrix}0 & \omega_b & 0 & 0 & 0\\ -\frac{K_1}{M} & -\frac{K_d}{M} & -\frac{K_2}{M} & 0 & \frac{K_3}{M}\\ \frac{K_4}{T'_{\mathrm{do}}} & 0 & -\frac{K_5}{T'_{\mathrm{do}}} & -\frac{1}{T'_{\mathrm{do}}} & -\frac{K_6}{T'_{\mathrm{do}}}\\ -\frac{K_aK_7}{T_A} & 0 & -\frac{K_AK_8}{T_A} & -\frac{1}{T_A} & -\frac{K_AK_9}{T_A}\\ -\frac{K_rK_{10}}{T_r} & 0 & -\frac{K_rK_{11}}{T_r} & 0 & -\frac{1+K_rK_{12}}{T_r}\end{bmatrix}\times\begin{bmatrix}\Delta\delta\\ \Delta\omega\\ \Delta E'_q\\ \Delta E_f\\ \Delta B_C\end{bmatrix}+\begin{bmatrix}0 & 0 & 0\\ \frac{1}{M} & 0 & 0\\ 0 & 0 & 0\\ 0 & \frac{K_A}{T_A} & 0\\ 0 & 0 & \frac{K_r}{T_r}\end{bmatrix}\begin{bmatrix}\Delta T_m\\ \Delta V_{\mathrm{ref}}\\ \Delta\omega\end{bmatrix}. \qquad (22)$$

The block diagram of the linearized dynamic model of the SMIB power system with FC-MCR is shown in Figure 13.

5. FC-MCR controller design using ICA

In this proposed method, the parameters of the FC-MCR controller are optimally adjusted for the dynamic stability of the entire system. Considering the fact that the selection of gains of output feedback for FC-MCR as a damping controller is a complicated optimization problem, to increase the system damping for electromechanical modes, a multi-objective function based on eigenvalues is considered which includes two separate objective functions that form a compound objective function with an appropriate weight ratio. The ICA algorithm is used to obtain optimum values for the objective function. The multi-objective function with an appropriate weight ratio is considered as follows:

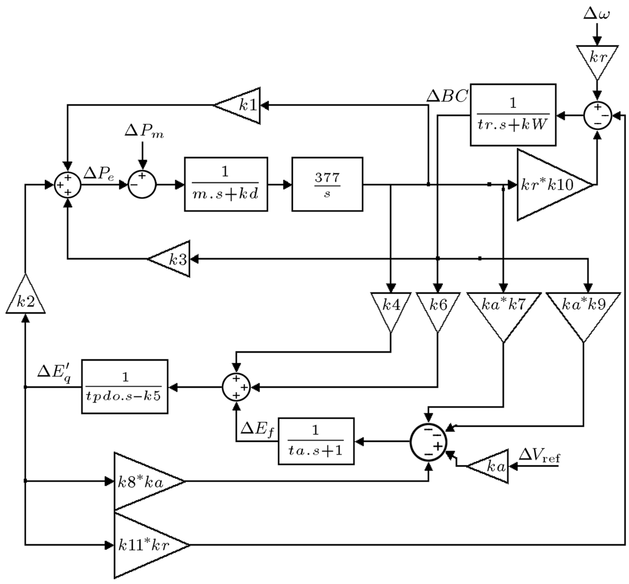

Figure 13. Phillips-Heffron model of SMIB power system with FC-MCR.

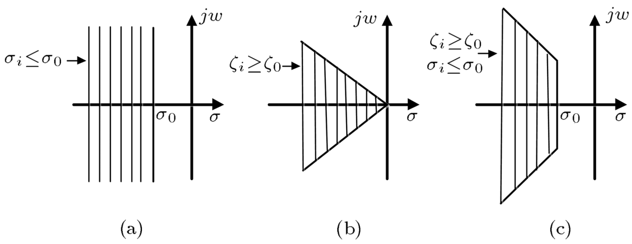

Figure 14. Region of eigenvalue location for the objective function.

$$J_1 = \sum_{j=1}^{\text{NP}} \sum_{\sigma_i \geq \sigma_0} (\sigma_0 - \sigma_i)^2,$$

$$J_2 = \sum_{j=1}^{\text{NP}} \sum_{\xi_i \leq \xi_0} (\xi_0 - \xi_i)^2,$$

$$J = J_1 + aj_2, \tag{23}$$

where $\sigma_{i,j}$ and $\zeta_{i,j}$ are the real part and damping ratio of the ith eigenvalue in the jth operating point, respectively. The value of α is equal to 10, and NP is equal to the number of operating points in the optimization problem. By considering J_1, the dominant eigenvalues are transferred to the left side of the line $s = \sigma_0$ in the S-plane, according to Figure 14(a). This provides relative stability in the system. Similarly, if we consider objective function, J_2, the maximum overshoot of eigenvalues becomes limited and eigenvalues are transmitted to the specified area, which is shown in Figure 14(b). Multi-purpose objective function, J, transmits the eigenvalues of the system to the specified area shown in Figure 14(c).

The designing problem is formulated as a constrained optimization problem where the constraints are as follows:

$$K_{\min} \leq K \leq K_{\max}, \qquad T_{1\min} \leq T_1 \leq T_{1\max},$$
$$T_{2\min} \leq T_2 \leq T_{2\max}, \qquad T_{3\min} \leq T_3 \leq T_{3\max},$$
$$T_{4\min} \leq T_4 \leq T_{4\max}. \tag{24}$$

The proposed method uses the ICA intelligent algorithm to solve the optimization problem to obtain the optimal set of control parameters. The objective function given in Eq. (24) takes place under different performance conditions of the system; the desired performance conditions are considered in Table 1.

Table 1. Loading condition.

Operating conditions	P (pu)	Q (pu)	X_L (pu)
Base case	0.8	0.2629	0.6
Case 1	0.8	0.2629	1.2
Case 2	0.4	0.1314	0.6
Case 3	0.4	0.1314	1.2
Case 4	1.2	0.3943	0.6
Case 5	1.2	0.3943	1.2

Table 2. The optimal parameter settings of the proposed controllers based on the different objective function.

Controller parameters	J_1	J_2	J
K	79.5052	97.2635	98.248
T_1	0.5584	0.6458	0.7874
T_2	0.0992	0.04	0.296
T_3	0.3957	0.1659	0.9395
T_4	0.7762	0.6088	0.54

In this work, the range of optimization parameters for K is selected between [1-100], and the range of parameters for T_1, T_2, T_3 and T_4 is selected between [0.01-1]. In order to force the proposed algorithm to achieve desirable responses, the number of countries, early empires, iteration steps of the algorithm, revolution rate, absorption coefficient, absorption angle coefficient, and damping rates are set to 80, 8, 30, 0.3, 2, 0.5 and 0.99, respectively. The proposed optimization algorithms have been implemented several times and, then, a set of optimal values is selected. The final values of the optimized parameters, with both single objective functions, J_1 and J_2, and the multi-objective function, J, are given in Table 2.

6. Simulation results

In order to demonstrate the effectiveness and robustness of the proposed controller against severe turbu-

Table 3. Eigenvalues and damping ratios of electromechanical modes with and without controller.

Operating conditiond	Type of controller			
	Without controller (damping ratio)	J_1 (damping ratio)	J_2 (damping ratio)	J (damping ratio)
Base Case	**$0.2572 \pm 4.9640i$, (-0.0517)** -5.5092, -3.4183 -94.8857	$-1.0308 \pm 5.1850i$, (0.195) -7.8629, -6.0251 -3.6018, -1.2584 -1.007, -94.8861	$-1.0650 \pm 5.2552i$, (0.198) -23.7673, -5.4895 -3.0285, -1.6677 -1.009, -94.8865	$-2.3442 \pm 7.1730i$, (0.31) $-1.5813 \pm 1.8401i$, (0.651) -5.1455, -1.6741 -1.018, -94.8867
Case 1	**$0.4414 \pm 4.9798i$, (-0.088)** $-5.2558 \pm 0.3026i$, (0.998) -94.0021	$-6.4118 \pm 5.1683i$, (0.778) $-2.0498 \pm 4.324i$, (0.428) -4.5729, -1.2555 -1.009, -94.0130	$-2.2824 \pm 4.6633i$, (0.439) $-5.3670 \pm 0.9645i$, (0.984) -21.0465, -1.6664 -1.012, -94.0262	$-4.2354 \pm 10.2156i$, (0.383) $-1.1368 \pm 1.9245i$, (0.508) -4.1800, -1.6780 -1.031, -94.0273
Case 2	**$0.3904 \pm 2.7480i$, (-0.14)** -3.2725, -1.4170 -98.6749	$-0.6603 \pm 2.7920i$, (0.23) -9.4974, -3.3654 -1.4510, -1.2038 -1.010, -98.6748	$-0.7301 \pm 2.8541i$, (0.247) -24.6316, -3.4037 -1.5012, -1.3792 -1.021, -98.6746	$-2.5343 \pm 3.4483i$, (0.592) $-1.2263 \pm 1.8284i$, (0.557) -1.4016, -1.7766 -1.022, -98.6776
Case 3	**$0.3991 \pm 3.0238i$, (-0.13)** -0.9325, -1.3473 -98.7806	$-0.5482 \pm 3.1674i$, (0.17) $-1.3649 \pm 0.0812i$, (0.998) -9.8332, -0.7858 -1.017, -98.7806	$-0.5593 \pm 3.2226i$, (0.171) -24.8029, -1.021 -0.7891, -1.3765 -1.6315, -98.7805	$-1.0590 \pm 3.5785i$, (0.283) $-1.9619 \pm 0.5736i$, (0.959) -1.3548, -0.9096 -1.020, -98.7809
Case 4	**$0.0235 \pm 6.9746i$, (-0.0033)** -11.9635, -3.9144 -88.8899	$-1.1453 \pm 7.3335i$, (0.154) $-9.7518 \pm 2.1716i$, (0.976) -4.2156, -1.2702 -1.005, -88.9033	$-1.2028 \pm 7.2571i$, (0.163) -21.6922, -13.1433 -3.6398, -1.6560 -1.006, -88.9199	$-2.5939 \pm 9.6474i$, (0.259) $-2.0183 \pm 2.0105i$, (0.708) -14.1865, -1.7176 -1.007, -88.9958
Case 5	**$0.0146 \pm 6.9483i$, (-0.0021)** -17.2419, -6.5269 -83.8250	$-13.4906 \pm 7.1507i$, (0.883) $-0.5140 \pm 6.4179i$, (0.079) -5.6577, -1.2871 -1.001, -83.9794	$-20.4422 \pm 9.7367i$, (0.902) $-0.5310 \pm 6.3715i$, (0.083) -6.4462, -1.6430 -1.001, -84.1714	$-22.7374 \pm 10.1016i$, (0.913) $-1.1714 \pm 5.1615i$, (0.221) -6.5699, -1.8466 -1.002, -84.1807

lence and the damping of oscillations caused by it, the power system, using the proposed model, is simulated in MATLAB software. To make sure that the obtained results are reliable, this simulation is evaluated with an eigenvalue analysis method and time domain nonlinear simulation. This is shown as follows.

6.1. Eigenvalue analysis

The electromechanical modes and the damping ratios obtained for all operating conditions, both with and without the proposed controllers in the system, are given in Table 3. When FC-MCR is not installed, it can be seen that some of the modes are poorly damped and, in some cases, unstable (highlighted in Table 3). It is also clear that system damping with the proposed J based tuned FC-MCR controller is significantly improved.

6.2. Nonlinear time-domain simulation

The single-machine infinite-bus system shown in Figure 7 is considered for nonlinear simulation studies. A 6-cycle, 3-phase fault at $t = 1$ s is occurred on the infinite bus under all loading conditions given in Table 1 to study the performance of the proposed controller. The performance of the controller, when the multi-objective function is used in the design, is compared to that of the controllers designed using the single objective functions, J_1 and J_2. The speed deviation, electric power deviation and susceptance deviation, based on the controller, under six different loading conditions, are shown in Figures 15-20. It can be seen that the ICA based FC-MCR controller tuned, using the multi-objective function, achieves good robust performance, provides superior damping in comparison with the other objective functions and greatly enhances the dynamic stability of the power systems.

7. Conclusion

In this paper, a state equation of a new FC-MCR compensator is produced and a transient stability performance improvement by a FC-MCR controller has been investigated. The stabilizers are tuned to

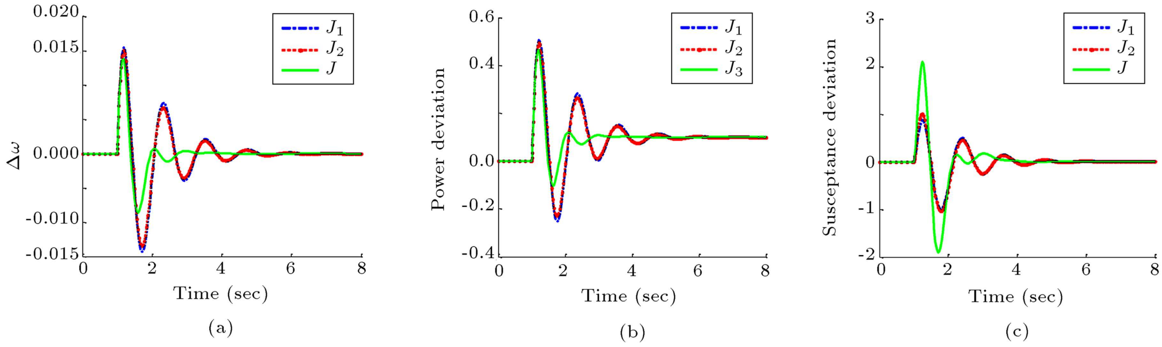

Figure 15. Dynamic responses for (a) $\Delta\omega$, (b) ΔP, and (c) ΔB_C with controller at base case loading condition.

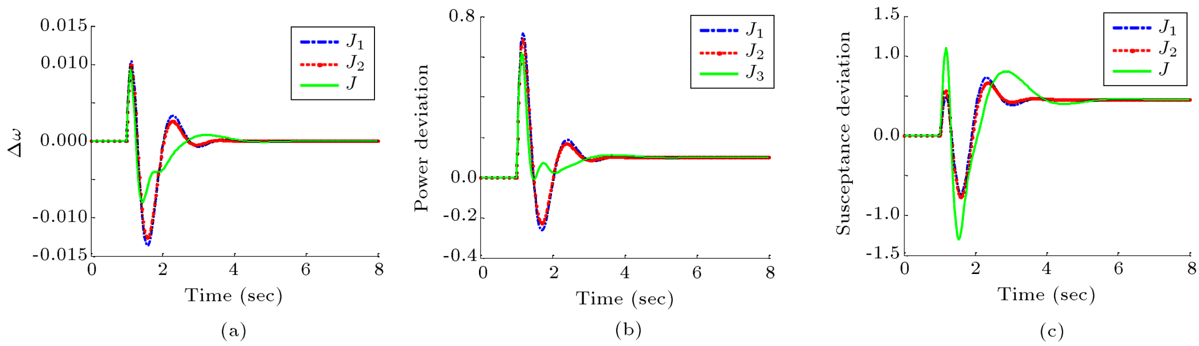

Figure 16. Dynamic responses for (a) $\Delta\omega$, (b) ΔP, and (c) ΔB_C with controller at case 1 loading condition.

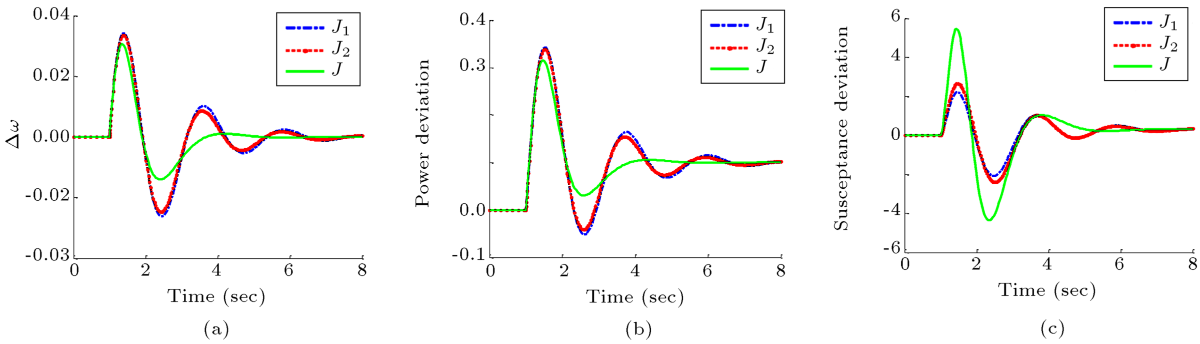

Figure 17. Dynamic responses for (a) $\Delta\omega$, (b) ΔP, and (c) ΔB_C with controller at case 2 loading condition.

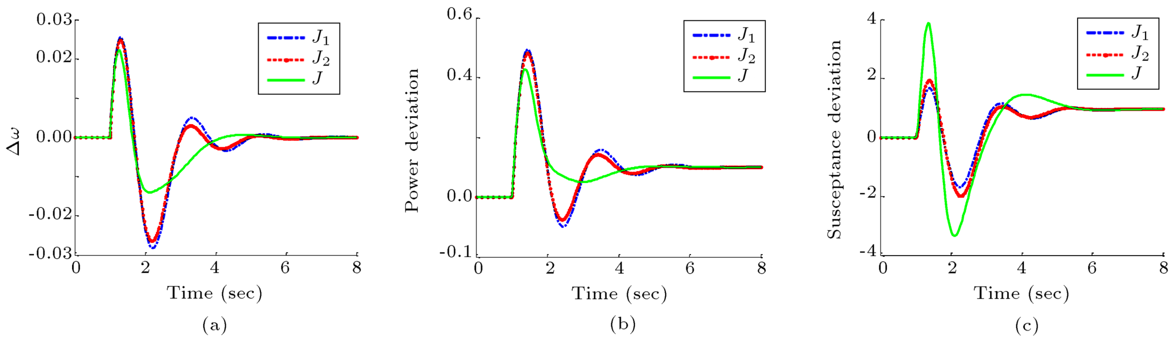

Figure 18. Dynamic responses for (a) $\Delta\omega$, (b) ΔP, and (c) ΔB_C with controller at case 3 loading condition.

simultaneously shift the undamped electromechanical modes of the machine to a prescribed zone in the s-plane. A multi-objective problem is formulated to optimize a composite set of objective functions, comprised of the damping factor and the damping ratio of the undamped electromechanical modes. The design problem of the controller is converted into an optimization problem, which is solved by an ICA technique with the eigenvalue-based multi-objective function. The effectiveness of the proposed FC-

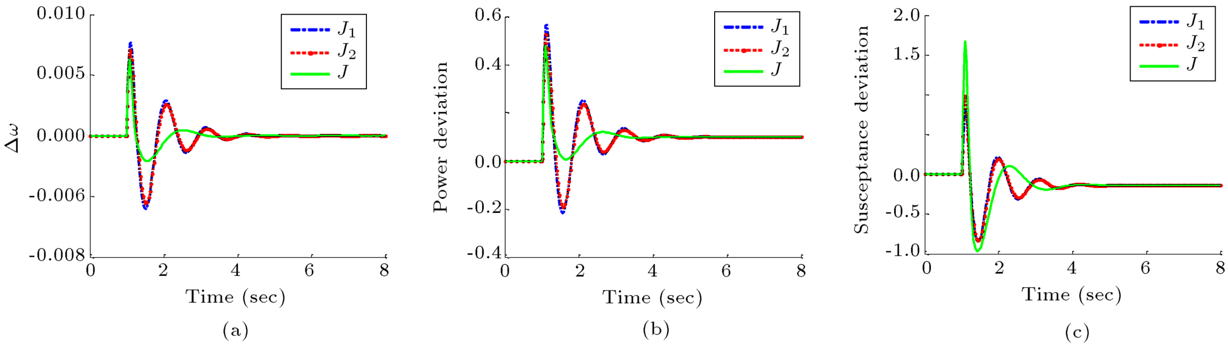

Figure 19. Dynamic responses for (a) $\Delta\omega$, (b) ΔP, and (c) ΔB_C with controller at case 4 loading condition.

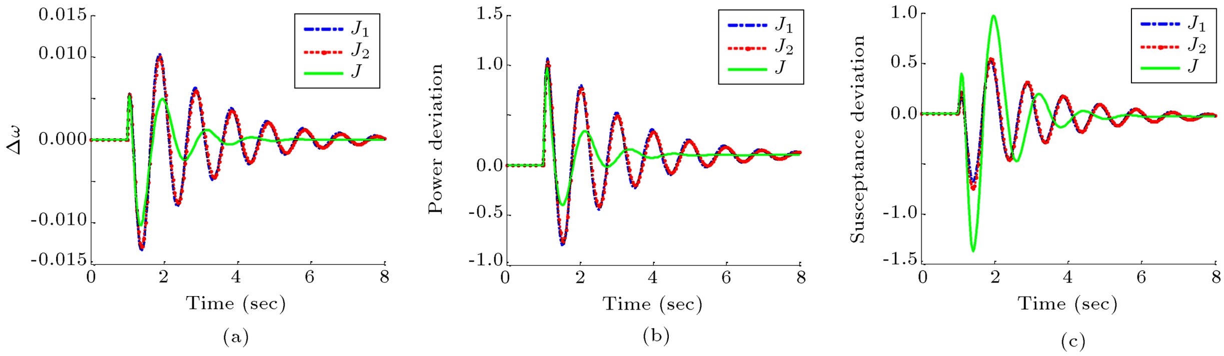

Figure 20. Dynamic responses for (a) $\Delta\omega$, (b) ΔP, and (c) ΔB_C with controller at case 5 loading condition.

MCR controllers for improving the transient stability performance of a power system is demonstrated by a weakly connected example power system subjected to different severe disturbances. The eigenvalue analysis and nonlinear time-domain simulation results show the effectiveness of the proposed controller, using the multi-objective function, and its ability to provide good damping of low frequency oscillations.

Nomenclature

B_0	Flux density of the OY windings
B_m	Maximum flux density of the CO windings
B_S	Flux density of knee saturation
H_m	Maximum magnetic field strength
I_C	Reactor current
S	Cross-section area of core
A	Gradient of knee saturation
φ_m	Maximum flux density
E'_q	Internal voltage behind transient reactance
E_{fd}	Equivalent excitation voltage
K	Proportional gain of the controller
K_A	Regulator gain
M	Machine inertia coefficient
P_e	Electric torque
P_m	Mechanical input power
ICA	Imperialist Competitive Algorithm
PSS	Power System Stabilizer
SMIB	Single Machine Infinite Bus
SVC	Static Var Compensator
Fc-MCR	Magnetically Controlled Reactor with Fixed Capacitor banks
T_1	Lead time constant of controller
T_2	Lag time constant of controller
T_3	Lead time constant of controller
T_4	Lag time constant of controller
T_A	Regulator time constant
T'_{do}	Time constant of excitation circuit
T_W	Washout time constant
T_s	Settling time of speed deviation
V_{pref}	Reference voltage
ω	Rotor speed
δ	Rotor angle
ΔP_e	Electrical power deviation

References

1. Al-Awami, A.T., Abdel-Magid, Y.L. and Abido, M.A. "A particle-swarm-based approach of power system stability enhancement with unified power flow controller", *Int. J. Elect. Power and Energy Syst*, **29**(3), pp. 251-259 (2007).
2. Anderson, P.M. and Fouad, A.A., *Power System Control and Stability*, Ames, IA: Iowa State University Press (1977).
3. Shayeghi, H., Shayanfar, H.A., Jalilzadeh, S. and Safari, A. "A PSO based unified power flow controller for damping of power system oscillations", *Energy Convers. and Manag.*, **50**(10), pp. 2583-2592 (2009).
4. Shayeghi, H., Shayanfar, H.A., Jalilzadeh, S. and Safari, A. "Design of output feedback UPFC controller for damping of electromechanical oscillations using PSO", *Energy Convers. and Manag.*, **50**(10), pp. 2554-2561 (2009).
5. Ajami, A. and Armaghan, M. "Application of multi-objective PSO algorithm for power system stability enhancement by means of SSSC", *Int. J. Comput. and Elect. Eng.*, **2**(5), pp. 838-845 (2010).
6. Abido, M.A. "Robust design of multimachine power system stabilizers using simulated annealing", *IEEE Trans. Energy Convers.*, **15**(3), pp. 297-304 (2000).
7. Chun liu, Ryuichi Yokoyama, Kaoru Koyanagi, Kwang Y. Lee, "PSS design for damping of inter-area power oscillations by coherency-based equivalent model", *Int. J. Elect. Power and Energy Syst.*, **26**(7), pp. 535-544 (2004).
8. Kundur, P., Klein, M., Rogers, G.J. and Zywno, M.S. "Application of power system stabilizers for enhancement of overall system stability", *IEEE Trans. Power Syst.*, **4**(2), pp. 614-626 (1989).
9. Keri, A.J.F., Lombard, X. and Edris, A.A. "Unified power flow controller: Modeling and analysis", *IEEE Trans. Power Syst.*, **14**(2), pp. 648-654 (1999).
10. Banaei, M.R. and Kami, A. "Interline power flow controller (IPFC) based damping recurrent neural network controllers for enhancing stability", *Energy Convers. and Manag.*, **52**(7), pp. 2629-2636 (2011).
11. Ding Lijie, Liu Yang, Miao Yiqun "Comparison of high capacity SVC and STATCOM in real power grid", *Int. Conf. Intellig. Comput. Tech. and Autom.*, **1**, pp. 993-997 (2010).
12. Abd-Elazim, S.M. and Ali, E.S. "Bacteria foraging optimization algorithm based SVC damping controller design for power system stability enhancement", *Int. J. Elect. Power and Energy Syst.*, **43**(1), pp. 933-940 (2012).
13. Abd-Elazim, S.M. and Ali, E.S. "Coordinated design of PSSs and SVC via bacteria foraging optimization algorithm in a multimachine power system", *Int. J. Elect. Power and Energy Syst.*, **41**(1), pp. 44-53 (2012).
14. Karymov, R.R. and Ebadian, M. "Comparison of Magnetically Controlled Reactor (MCR) and Thyristor Controlled Reactor (TCR) from harmonics point of view", *Int. J. Elect. Power and Energy Syst.*, **29**(3), pp. 191-198 (2007).
15. Ghanizadeh, R., Delbari, M. and Ebadian, M. "Matimaticall modeling and harmonics optimization of a multi-level magnetically controlled reactor with harmony search algorithm", *Int. Review Mod. and Simulat.*, **5**(4), pp. 1858-1866 (2012).
16. Ebadian, M. and Samadi, A.A. "High order harmonics reduction in Magnetically Controlled Reactor (MCR)", *Int. J. Elect. Eng*, **6**(3), pp. 519-525 (2009).
17. Ghanizadeh, R., Ebadian, M. and Golkar, M.A. "Performance comparison of a new compensator based on magnetically controlled reactor and Static Var Compensator (SVC)", *Int. Review Mod. and Simulat.*, **5**(4), pp. 1664-1671 (2012).
18. Ebadin, M. and Dstyar, F. "Performance comparison of transient behaviors of magnetically and thyristor-controlled reactors", *Elect. Power Component and Syst.*, **38**(1), pp. 85-99 (2009).
19. Ebadian, M., Ghanizadeh, R. and Delbari, M. "Assignment of Magnetically Controlled Reactor (MCR) parameters considering minimization of power losses", *Int. Review Mod. and Simulat.*, **5**(1), pp. 517-524 (2012).
20. Lucas, C., Nasiri-Gheidari, Z. and Tootoonchian, F. "Application of an imperialist competitive algorithm to the design of a linear induction motor", *Energy Convers. and Manag*, **51**(7), pp. 1407-1411 (2010).
21. Atashpaz-Gargari, E. and Lucas, C. "Imperialist competitive algorithm an algorithm for optimization inspired by imperialist competition", *IEEE Cong. on Evolut. Comput.*, pp. 4661-4667 (2007).
22. Nazari-Shirkouhi, S., Eivazy, H., Ghodsi, R., Rezaie, K. and Atashpaz-Gargari, E. "Solving the integrated product mix-outsourcing problem using the imperialist competetive algorithm", *Expert Syst. with Applicat.*, **37**(12), pp. 7615-7626 (2010).
23. Jahani, R., Hosseinzadeh, A., Gharegozi, A. and Mohammad Abadi, M. "ICA-based allocation of DGs in a distribution system", *Amer. J. Scientific Research*, **13**(33), pp. 64-75 (2011).
24. Atashpaz Gargari, E., Hashemzadeh, F., Rajabioun R. and Lucas, C. "Imperialist competitive algorithm: A novel approach for PID controller design in MIMO distillation column process", *Int. J. Int. Computing and Cybern (IJICC)*, **1**(3), pp. 337-355 (2008).

Appendix

The test system parameter are:

Generator:
$M = 8$ MJ/MVA, $T'_{\mathrm{do}} = 5.044$,
$X_d = 1$ pu, $X'_d = 0.3$ pu, $D = 4$.

Excitation system:
$K_A = 80$, $T_A = 0.05$ s.

Transformers:
$X_T = 0.1$ pu, $X_{\mathrm{SDT}} = 0.1$ pu.

Transmission line:
$X_L = 0.6$ pu.

FC_MCR parameters:
$K_r = 1$, $T_r = 0.3$.

Biographies

Reza Ghanizadeh was born in Mianeh, Iran, in 1987. He received an associate degree in Electrical Engineering from Tabriz College of Technology in 2007, and his BS degree in Electrical Engineering from the Islamic Azad University, Ardabil, Iran, in 2009. He obtained his MS degree in 2012 from the University of Birjand, Iran, where he is currently a PhD degree student in the Department of Power Engineering. His research interests are power system stability, reactive power control in transmission and distribution systems, power quality studies and FACTS devices.

Mahmoud Ebadian received his BS degree in Electrical Engineering from Ferdowsi University, Mashhad, Iran, in 1991, his MS degree from K. N. Toosi University of Technology, Tehran, Iran, in 1996, and his PhD degree from Moscow Power Engineering Institute, the Russian Federation, in 2006. He is currently Associate Professor in the Department of Power Engineering at the University of Birjand, South Khorassan, Iran. His research interests include voltage colapse, voltage stability and FACTS.

Masoud Aliakbar Golkar was born in Tehran, Iran, in 1954. He received his BS degree from Sharif University of Technology, Tehran, Iran, in 1977, his MS degree from Oklahoma State University, USA, in 1979, and his PhD degree from Imperial College of Science, Technology and Medicine, University of London, UK, in 1986, all in Electrical Engineering (Power Systems). He was Senior Lecturer at Curtin University of Technology in Malaysia from January 2002 to July 2005, and is currently Professor in the Department of Power Engineering at K. N. Toosi University, Tehran, Iran.

Ahad Jahandideh Shendi was born in Shabestar, Iran, in 1985. He received BS and MS degrees in Electrical Engineering from Azad University, Iran, in 2008 and 2012, respectively. His research interests are power system stability, reactive power control in transmission & distribution systems, power quality studies and FACTS devices.